



Dipole-mode and scissors-mode oscillations of a dipolar supersolid

Luis E. Young-S. ^{1,*} and S. K. Adhikari ^{2,†}

¹*Grupo de Modelado Computacional, Facultad de Ciencias Exactas y Naturales, Universidad de Cartagena, 130014 Cartagena, Bolivar, Colombia*

²*Instituto de Física Teórica, Universidade Estadual Paulista, 01.140-070 São Paulo, São Paulo, Brazil*



(Received 21 February 2023; revised 18 April 2023; accepted 10 May 2023; published 30 May 2023)

We study dipole-mode and scissors-mode oscillations of a harmonically trapped dipolar supersolid, composed of dipolar droplets arranged on a one-dimensional (1D) or a 2D lattice, to establish the robustness of its crystalline structure under translation and rotation, using a beyond-mean-field model including a Lee-Huang-Yang interaction. The dipolar atoms are polarized in the z direction with the supersolid crystalline structure lying in the x - y plane. A stable dipole-mode oscillation is possible in the case of both quasi-1D and quasi-2D dipolar supersolids, whereas a sustained angular scissors-mode oscillation is possible only in the case of a quasi-1D dipolar supersolid between a maximum and a minimum of trap anisotropy in the x - y plane. In both cases there is no visible deformation of the crystalline structure of the dipolar supersolid during the oscillation. The theoretical estimate of the scissors-mode-oscillation frequency is in good agreement with the present results and the agreement improves with an increase in the number of droplets in the supersolid and also with an increase in the confining trap frequencies. The results of this study can be tested experimentally with present knowhow.

DOI: [10.1103/PhysRevA.107.053318](https://doi.org/10.1103/PhysRevA.107.053318)

I. INTRODUCTION

A supersolid [1–6], or a superfluid solid, is a quantum state of matter simultaneously possessing the properties of both a solid and a superfluid. Hence, a supersolid has a spatially periodic crystalline structure as a solid, breaking continuous translational invariance, and also enjoys frictionless flow like a superfluid, breaking continuous gauge invariance. The pioneering search of supersolidity in ultracold ^4He [7] was not successful [8]. Later, there had been theoretical suggestions for creating a supersolid in a Bose-Einstein condensate (BEC) with finite-range atomic interaction [9], or specifically, in a dipolar BEC [10–12], and also in a spin-orbit-coupled (SOC) spinor BEC [13]. The study of supersolids has recently gained new momentum among research workers in various fields, after the experimental observation of supersolids in a quasi-one-dimensional (quasi-1D) [14–17] and quasi-2D [18] dipolar BEC and in a quasi-1D SOC pseudospin- $\frac{1}{2}$ spinor BEC [19,20].

Recently, in the pursuit of a supersolid, a spatially periodic state with a 1D stripe pattern in density was observed in an SOC pseudospin- $\frac{1}{2}$ BEC of ^{23}Na [19] and ^{87}Rb [20] atoms. Later, in theoretical studies of quasi-2D SOC spin-1 [21,22], spin-2 [23], and pseudospin- $\frac{1}{2}$ [24] spinor BECs, the formation of stripe and square- and hexagonal-lattice [13,19] patterns in density was demonstrated.

In a different context, in a strongly dipolar BEC, for the number of atoms N beyond a critical value, high-density droplets were observed experimentally in a trapped BEC of ^{164}Dy [25,26] and ^{168}Er [27] atoms and studied theoretically [28,29]. In a quasi-1D trapped BEC of ^{164}Dy [14,30,31],

^{162}Dy [15,16,32], and ^{166}Er [14,31] atoms, with a large N , a dipolar supersolid in the form of a spatially periodic arrangement of droplets in a straight line was observed in different experiments [14–17] and also was studied theoretically [17,33]. In a quasi-2D trapped BEC of ^{164}Dy atoms, a dipolar supersolid in the form of a spatially periodic arrangement of droplets on a hexagonal lattice was observed experimentally [18] and established theoretically [34–38]. In a trapped quasi-2D dipolar BEC, the formation of honeycomb-lattice, stripe, square-lattice, and other periodic patterns in density were also found [34,35,38–41] in theoretical studies.

In the framework of a mean-field model employing the Gross-Pitaevskii (GP) equation, a dipolar BEC collapses for a strong dipolar interaction beyond a critical value [42] and a Lee-Huang-Yang [43] (LHY) beyond-mean-field interaction [44,45] is necessary in theoretical studies to stabilize a strongly dipolar droplet against collapse [12]. As the number of atoms N in a trapped dipolar BEC is increased, so that the density of atoms reaches a critical value, due to the dipolar attraction, the condensate shrinks to a very small size. However, it cannot collapse due to the LHY interaction and a droplet is formed [25,26] in the case of an appropriate mixture of contact and dipolar interactions. The size of the droplet is much smaller than the harmonic oscillator trap lengths. Such droplets can accommodate a maximum number of atoms [28] for a given harmonic trap frequencies so as to attain a critical density of atoms in the condensate. As the number of atoms is increased further in the dipolar BEC, multiple droplets are generated and due to an interplay between the dipolar repulsion in the x - y plane and the external trapping potential, a supersolidlike arrangement of droplets on a spatially periodic lattice emerges as the minimum-energy state [46–48]. In spite of the name droplet, the present dipolar BEC droplets in a strong trap are different from recently observed [49,50] nondipolar binary BEC droplets in free space. Nevertheless,

*lyoung@unicartagena.edu.co

†sk.adhikari@unesp.br; professores.ift.unesp.br/sk.adhikari/

in both cases, the collapse is arrested [51] by a beyond-mean-field LHY interaction [43].

Although there have been many theoretical investigations of the statics of dipolar supersolids [33,52–63], there have hardly been any direct studies of the dynamics. Linear dipole-mode and angular scissors-mode oscillations of a BEC are earmarks of superfluidity. Scissors-mode oscillation of a single droplet [64] as well as a quasi-1D dipolar supersolid [65] has been studied experimentally and theoretically [66]. In Refs. [65,66] the authors studied the variation of scissors-mode-oscillation frequency with a variation of the strength of the dipolar interaction relative to that of the contact interaction. In the present study we consider an evolution of the scissors-mode oscillation with a variation of trap frequency while the trap passes from a quasi-1D to a quasi-2D type. Hence the two studies are complementary to each other. In the case of a dipolar supersolid and dipole-mode and scissors-mode oscillations, without any distortion of the lattice structure of droplets, tests of both the superfluidity and the robustness of the crystalline structure of the dipolar supersolid under translation and rotation hence confirm the supersolidity of these states.

Inspired by the experimental study of Ref. [65], to test the superfluidity and robustness of a dipolar supersolid, in this paper we study the linear dipole-mode-oscillation and angular scissors-mode-oscillation dynamics of a harmonically trapped dipolar supersolid. The dipole-mode oscillation of a quasi-1D or quasi-2D dipolar supersolid is studied by employing real-time propagation by giving a sudden translation of the harmonic trap in the x direction. To study the angular scissors-mode oscillation of a quasi-1D dipolar supersolid, with an asymmetric trapping potential in the x - y plane, a sudden rotation of the harmonic trap in the z direction is applied. In both cases a continuous steady oscillation of the dipolar supersolid was confirmed without any visible distortion of the crystalline structure, thus establishing the superfluidity and the robustness of the crystalline structure of the dipolar supersolid. Although the theoretical estimate of the scissors-mode-oscillation frequency $\omega_{\text{th}} = \sqrt{\omega_x^2 + \omega_y^2}$ [67], where ω_x and ω_y are the angular trap frequencies in the x and y directions, respectively, is a good approximation to the actual frequency of oscillation, the agreement improves as the number of droplets in the dipolar supersolid increases or as the confining trap becomes stronger. For a sustained periodic scissors-mode oscillation, the trap asymmetry in the x - y plane should lie between an upper and a lower limit. As the asymmetry is reduced beyond the lower limit or increased above the upper limit, the periodic simple-harmonic scissors-mode oscillation becomes an irregular one. No sustained scissors-mode oscillation was found for a quasi-2D dipolar supersolid with a hexagonal- or square-lattice structure. The linear dipole-mode oscillation in the x direction is simple harmonic and takes place with the frequency of the trap ω_x . While studying the scissors-mode oscillation of a quasi-1D dipolar supersolid we keep ω_x and ω_z fixed maintaining $\omega_z \gg \omega_x$ and vary ω_y such that $\omega_y > \omega_x$, thus generating a trap with asymmetry in the x - y plane as required to initiate the scissors-mode oscillation. As ω_y increases from a small value to a value larger than ω_z the trap changes from a quasi-2D type to a quasi-1D type. In this fashion we study the evolution of

the scissors-mode oscillation of a quasi-1D dipolar supersolid in both types of trap; in all cases the numerical frequency of the scissors-mode oscillation was smaller than its theoretical estimate.

In Sec. II we consider the beyond-mean-field model including the LHY interaction. We also present the appropriate energy functional, a minimization of which leads to this model. In Sec. III we present numerical results for dipole-mode oscillation of quasi-1D three-droplet and quasi-2D nine-droplet dipolar supersolids of ^{164}Dy atoms after a sudden displacement of the trap. We also present results for angular scissors-mode oscillation of quasi-1D three-droplet and five-droplet dipolar dipolar supersolids. A variation of the scissors-mode frequency with ω_y , as the trap evolves from a quasi-2D to a quasi-1D type, is also studied. A breakdown of the scissors-mode oscillation of a nine-droplet quasi-2D square-lattice and a seven-droplet triangular-lattice dipolar supersolid is also demonstrated. Finally, in Sec. IV we present a summary of our findings.

II. BEYOND-MEAN-FIELD MODEL

We consider a BEC of N dipolar atoms, of mass m each, polarized along the z axis, interacting through the atomic contact and dipolar interactions [68–70]

$$V(\mathbf{R}) = \frac{\mu_0 \mu^2}{4\pi} U_{\text{dd}}(\mathbf{R}) + \frac{4\pi \hbar^2 a}{m} \delta(\mathbf{r} - \mathbf{r}'), \quad (1)$$

$$U_{\text{dd}}(\mathbf{R}) = \frac{1 - 3 \cos^2 \theta}{|\mathbf{r} - \mathbf{r}'|^3}, \quad (2)$$

where μ is the magnetic dipole moment of each atom, μ_0 is the permeability of the vacuum, and a is the scattering length. Here $\mathbf{r} \equiv \{\mathbf{x}, \mathbf{y}, \mathbf{z}\}$ and $\mathbf{r}' \equiv \{\mathbf{x}', \mathbf{y}', \mathbf{z}'\}$ are the positions of the two interacting dipolar atoms and θ is the angle made by $\mathbf{R} \equiv \mathbf{r} - \mathbf{r}'$ with the polarization z direction. In analogy with the scattering length, the dipolar length a_{dd} determines the strength of the dipolar interaction

$$a_{\text{dd}} = \frac{\mu_0 \mu^2 m}{12\pi \hbar^2}. \quad (3)$$

The dimensionless ratio

$$\varepsilon_{\text{dd}} \equiv \frac{a_{\text{dd}}}{a} \quad (4)$$

determines the strength of the dipolar interaction relative to the contact interaction and controls many properties of a dipolar BEC.

In this paper we base our study on a 3D beyond-mean-field model including the LHY interaction. The formation of a lattice of droplets is described by the 3D beyond-mean-field GP equation including the LHY interaction [29,36,68–70]

$$i\hbar \frac{\partial \psi(\mathbf{r}, t)}{\partial t} = \left(-\frac{\hbar^2}{2m} \nabla^2 + U(\mathbf{r}) + \frac{4\pi \hbar^2}{m} aN |\psi(\mathbf{r}, t)|^2 \right. \\ \left. + \frac{3\hbar^2}{m} a_{\text{dd}} N \int U_{\text{dd}}(\mathbf{R}) |\psi(\mathbf{r}', t)|^2 d\mathbf{r}' \right. \\ \left. + \frac{\gamma_{\text{LHY}} \hbar^2}{m} N^{3/2} |\psi(\mathbf{r}, t)|^3 \right) \psi(\mathbf{r}, t), \quad (5)$$

$$U(\mathbf{r}) = \frac{1}{2} m (\omega_x^2 x^2 + \omega_y^2 y^2 + \omega_z^2 z^2), \quad (6)$$

where ω_x , ω_y , and ω_z are the angular frequencies in the x , y , and z directions, respectively, and the wave function is normalized as $\int |\psi(\mathbf{r}, t)|^2 d\mathbf{r} = 1$. The coefficient of the beyond-mean-field LHY interaction γ_{LHY} is given by [29,44,45]

$$\gamma_{\text{LHY}} = \frac{128}{3} \sqrt{\pi} a^5 Q_5(\varepsilon_{\text{dd}}), \quad (7)$$

where the auxiliary function $Q_5(\varepsilon_{\text{dd}})$ is given by

$$Q_5(\varepsilon_{\text{dd}}) = \int_0^1 dx (1 - \varepsilon_{\text{dd}} + 3x^2 \varepsilon_{\text{dd}})^{5/2}. \quad (8)$$

This function can be evaluated as [29]

$$Q_5(\varepsilon_{\text{dd}}) = \frac{(3\varepsilon_{\text{dd}})^{5/2}}{48} \Re \left[(8 + 26\eta + 33\eta^2) \sqrt{1 + \eta} + 15\eta^3 \ln \left(\frac{1 + \sqrt{1 + \eta}}{\sqrt{\eta}} \right) \right], \quad \eta = \frac{1 - \varepsilon_{\text{dd}}}{3\varepsilon_{\text{dd}}}, \quad (9)$$

where \Re denotes the real part.

Equation (5) can be reduced to the dimensionless form by scaling lengths in units of $l = \sqrt{\hbar/m\omega_z}$, time in units of ω_z^{-1} , angular frequency in units of ω_z , energy in units of $\hbar\omega_z$, and density $|\psi|^2$ in units of l^{-3} ,

$$i \frac{\partial \psi(\mathbf{r}, t)}{\partial t} = \left(-\frac{1}{2} \nabla^2 + U(\mathbf{r}) + 4\pi a N |\psi(\mathbf{r}, t)|^2 + 3a_{\text{dd}} N \int U_{\text{dd}}(\mathbf{R}) |\psi(\mathbf{r}', t)|^2 d\mathbf{r}' + \gamma_{\text{LHY}} N^{3/2} |\psi(\mathbf{r}, t)|^3 \right) \psi(\mathbf{r}, t), \quad (10)$$

$$U(\mathbf{r}) = \frac{1}{2} (\omega_x^2 x^2 + \omega_y^2 y^2 + z^2). \quad (11)$$

Here and in the following, without any risk of confusion, unless otherwise indicated, all variables are scaled and represented by the same symbols as the unscaled variables.

Equation (10) can also be obtained from the variational rule

$$i \frac{\partial \psi}{\partial t} = \frac{\delta E}{\delta \psi^*} \quad (12)$$

with the energy functional (energy per atom)

$$E = \frac{1}{2} \int d\mathbf{r} \left(|\nabla \psi(\mathbf{r})|^2 + (\omega_x^2 x^2 + \omega_y^2 y^2 + z^2) |\psi(\mathbf{r})|^2 + 3a_{\text{dd}} N |\psi(\mathbf{r})|^2 \int U_{\text{dd}}(\mathbf{R}) |\psi(\mathbf{r}')|^2 d\mathbf{r}' + 4\pi N a |\psi(\mathbf{r})|^4 + \frac{4\gamma_{\text{LHY}}}{5} N^{3/2} |\psi(\mathbf{r})|^5 \right) \quad (13)$$

for a stationary state. First, a stationary quasi-1D or a quasi-2D dipolar supersolid state is generated by solving Eq. (10) by imaginary-time propagation. To study the dipole-mode oscillation, we perform real-time propagation with the space-translated potential

$$U(\mathbf{r}) = \frac{1}{2} [\omega_x^2 (x - x_0)^2 + \omega_y^2 y^2 + z^2] \quad (14)$$

and using the stationary state as the initial function, where x_0 is the space translation in the x direction. In this case

a nondipolar BEC executes the simple-harmonic oscillation $x(t) = x_0 \cos(\omega_x t)$ in the x direction without any distortion with angular frequency ω_x indicating superfluidity.

To study the angular scissors-mode oscillation of a quasi-1D supersolid state in the x - y plane, the real-time propagation is executed with the space-rotated trap

$$U(\mathbf{r}) = \frac{1}{2} [\omega_x^2 (x \cos \theta_0 + y \sin \theta_0)^2 + \omega_y^2 (-x \sin \theta_0 + y \cos \theta_0)^2 + z^2], \quad (15)$$

employing the stationary state as the initial function, where θ_0 is the angle of rotation of the potential in the polarization z direction. For a sufficiently large asymmetry of the trap in the x - y plane, a (superfluid) BEC, in the Thomas-Fermi regime, obeying the hydrodynamic equations of superfluids, will execute sustained periodic scissors-mode oscillation $\theta(t) = \theta_0 \cos(\omega_{\text{th}} t)$ with the frequency $\omega_{\text{th}} = \sqrt{\omega_x^2 + \omega_y^2}$ [67,71]. A sustained angular oscillation with the frequency ω_{th} signals superfluidity. In the opposite collisionless regime, distinct frequencies $|\omega_x \pm \omega_y|$ survive [67]. Because of the asymmetry of the dipolar interaction, say, in the x - z plane, it is also possible to have a spontaneous scissors-mode oscillation [64] of a dipolar BEC in this plane with a circularly symmetric trapping potential. The emergent circularly asymmetric dipolar BEC will naturally point in the z direction in this case and, if angularly displaced, can execute a scissors-mode oscillation in the x - z plane. That scissors-mode oscillation is typically different from the present scissors-mode oscillation generated in a circularly asymmetric trap in the x - y plane.

To generate a quasi-1D dipolar supersolid in the x direction we need to take $\omega_x \ll \omega_y$, 1; to generate a quasi-2D dipolar supersolid in the x - y plane we will take $\omega_x, \omega_y \ll 1$. (The angular frequencies are expressed in units of the angular frequency in the z direction, which in dimensionless units is 1.) In the case of dipole-mode oscillation we will consider both a quasi-1D and a quasi-2D dipolar supersolid and in the case of scissors-mode oscillation we will mostly study only a quasi-1D dipolar supersolid. We could not find any sustained scissors-mode oscillation in the case of a quasi-2D dipolar supersolid for any sets of parameters.

III. NUMERICAL RESULTS

To study the oscillation dynamics of a dipolar supersolid we solve the partial differential beyond-mean-field GP equation (10), numerically, using FORTRAN C programs [69] or their open-multiprocessing versions [72,73], employing the split-time-step Crank-Nicolson method using the imaginary-time propagation rule [74]. Because of the divergent $1/|\mathbf{R}|^3$ term in the dipolar potential (1), it is problematic to treat numerically the nonlocal dipolar interaction integral in the beyond-mean-field model (10) in configuration space. To circumvent the problem, this term is evaluated in the momentum \mathbf{k} space by a Fourier transformation using a convolution identity as [69]

$$\int d\mathbf{r}' U_{\text{dd}}(\mathbf{R}) n(\mathbf{r}') = \int \frac{d\mathbf{k}}{(2\pi)^3} e^{-i\mathbf{k}\cdot\mathbf{r}} \tilde{V}_{\text{dd}}(\mathbf{k}) \tilde{n}(\mathbf{k}), \quad (16)$$

where $n(\mathbf{r}) \equiv |\psi(\mathbf{r})|^2$ and $\tilde{V}_{\text{dd}}(\mathbf{k})$ and $\tilde{n}(\mathbf{k})$ are respective Fourier transforms. This is advantageous numerically due to

the smooth behavior of this term in momentum space. The Fourier transformation of the dipolar potential $\tilde{V}_{\text{dd}}(\mathbf{k})$ can be found analytically [69] enhancing the accuracy of the numerical procedure. After solving the problem in momentum space, a backward Fourier transformation provides the desired solution in configuration space.

For the appearance of a supersolid droplet lattice we need a strongly dipolar atom with $a_{\text{dd}} > a$ [25]. The system becomes repulsive for $a_{\text{dd}} < a$, while the system is necessarily a superfluid, and no droplets can be formed. Instead of presenting results only in dimensionless units, we also relate our results to the recent experimental [18,65] and related theoretical [36] studies on supersolid formation in a dipolar BEC of ^{164}Dy atoms. Although $a_{\text{dd}} = 130.8a_0$ for ^{164}Dy atoms, where a_0 is the Bohr radius, we have a certain flexibility in fixing the scattering length a , as the scattering length can be modified by the Feshbach resonance technique by manipulating an external electromagnetic field. As in our previous studies [39,40], we take $a = 85a_0$, which is close to its experimental estimate $a = (92 \pm 8)a_0$ [75]. With the reduction of contact repulsion, this choice has the advantage of slightly increasing the net attraction, which will facilitate the formation of the dipolar droplets. Consequently, we use $a = 85a_0$ in all calculations of this paper. Other studies of quantum droplets in a quasi-2D dipolar BEC used nearby values of scattering lengths, e.g., $a = 88a_0$ [18,36] and $a = 70a_0$ [37], always smaller than its experimental estimate to facilitate the formation of droplets and the droplet lattice.

In this study the trap frequencies in the x and z directions are taken as $\omega_x = \frac{33}{167}$ and $\omega_z = 1$ for trap A, as in a recent experimental [18] and related theoretical [36] investigations on hexagonal-lattice crystallization of droplets. For dysprosium atoms $m(^{164}\text{Dy}) \approx 164 \times 1.66054 \times 10^{-27}$ kg, $\hbar = 1.0545718 \times 10^{-34}$ m² kg/s, and $\omega_z = 2\pi \times 167$ Hz; consequently, the unit of length $l = \sqrt{\hbar/m\omega_z} = 0.6075$ μm . To find the dependence of the scissors-mode-oscillation frequency on the trapping frequency, we also considered the frequencies (for trap B) $\omega_x = \frac{23}{90}$ and $\omega_z = 1$, as in a recent experimental study of scissors-mode oscillation of a quasi-1D dipolar supersolid [65]; in that case $l = 0.8275$ μm . In both cases the trap frequency in the y direction ω_y will be varied to generate an appropriate quasi-1D or quasi-2D trap.

A. Dipole-mode oscillation of a quasi-1D and a quasi-2D supersolid

To prepare a quasi-1D dipolar supersolid for the investigation of dynamics, we consider 20 000 ^{164}Dy atoms in the quasi-1D trap A with $\omega_x = \frac{33}{167}$, $\omega_y = \frac{110}{167}$, and $\omega_z = 1$. The dipolar BEC crystallizes in a three-droplet state along the x axis. The converged final state in this case can be obtained by imaginary-time simulation using an initial Gaussian wave function. However, the convergence is quicker if we use an analytic wave function for a few droplets (three or five) periodically arranged in the x direction with a fixed mutual separation and symmetrically placed around the occupied $x = 0$ site as in Ref. [39] and we will take such an initial state in the present study. A contour plot of the $z = 0$ and $y = 0$ sections of the 3D density $|\psi(x, y, 0)|^2$ (left side) and $|\psi(x, 0, z)|^2$ (right side) is shown in Fig. 1(a) with

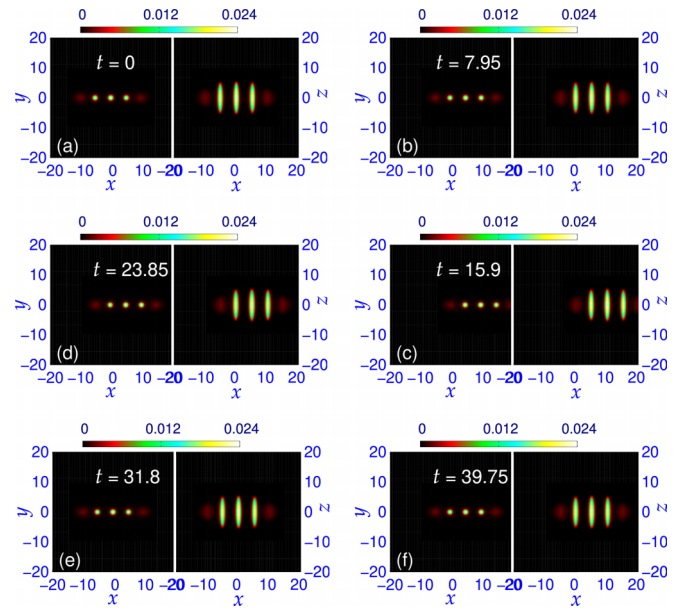


FIG. 1. Contour plot of density $|\psi(x, y, 0)|^2$ (left side of each panel) and $|\psi(x, 0, z)|^2$ (right side of each panel) of the quasi-1D three-droplet supersolid of $N = 20\,000$ ^{164}Dy atoms executing linear dipole-mode oscillation in trap A at times (a) $t = 0$, (b) $t = 7.95$, (c) $t = 15.9$, (d) $t = 23.85$, (e) $t = 31.8$, and (f) $t = 39.75$. The trap frequencies are $\omega_x = \frac{33}{167}$, $\omega_y = \frac{110}{167}$, and $\omega_z = 1$. Displayed results in all figures [except Fig. 5(a)] are dimensionless. The unit of length is $l = 0.6075$ μm and unit of time 0.953 ms.

three droplets placed symmetrically around $x = 0$ (a parity-symmetric state).

To study the dipole-mode oscillation, we consider the above-mentioned quasi-1D three-droplet dipolar supersolid in trap A [18,36], displaced in the x direction over a distance of $x_0 = 5$ [see Eq. (14)]. For both quasi-1D and quasi-2D dipole-mode oscillations (studied in the following), the initial configuration is the stationary state obtained by imaginary-time propagation and the dynamics is studied by real-time simulation replacing the original symmetric trap (11) by the displaced trap (14) with $x_0 = 5$ at $t = 0$. Due to the linear displacement of the trap in the x direction, the dipolar supersolid will execute sustained dipole-mode oscillation in the x direction with an amplitude of 5. In Fig. 2(a) we compare the time evolution of position x of the central droplet with its theoretical prediction of periodic oscillation with the trap frequency ω_x . The present period of oscillation $T = 31.8$ compares well with the theoretical period $T \equiv 2\pi/\omega_x = 31.7967$. The energy of the oscillating supersolid also executes a steady simple-harmonic oscillation as shown in Fig. 2(b). The frequency of energy oscillation is double that of the frequency of position oscillation. The dependence of the energy of the oscillating supersolid with time is important as it can be calculated much more accurately than the position of the supersolid and any deviation from the expected simple-harmonic oscillation of energy signals a breakdown of the expected dipole-mode and scissors-mode oscillations, indicating either a distortion of the supersolid or the destruction or absence of superfluidity during oscillation or both (see Fig. 9).

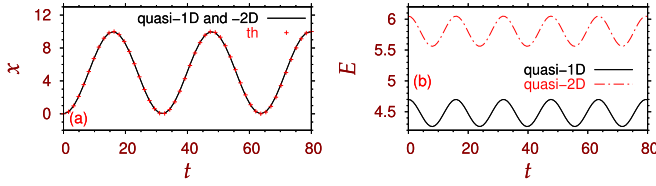


FIG. 2. (a) Linear displacement x of the central droplet versus time t of a quasi-1D three-droplet supersolid of $N = 20\,000$ ^{164}Dy atoms or of a quasi-2D nine-droplet supersolid of $N = 60\,000$ ^{164}Dy atoms executing dipole-mode oscillation in the x direction as obtained by real-time propagation fitted to the theoretical prediction $\cos(\omega_x t)$ (th). The oscillation is started by a linear displacement of $x_0 = 5$ of trap A at $t = 0$ [see Eq. (14)]. (b) Energy E versus time t during this dipole-mode oscillation. For the quasi-1D case, the angular frequency $\omega_x = \frac{110}{167}$ and for quasi-2D case $\omega_x = \frac{33}{167}$. The other parameters are $\omega_x = \frac{33}{167}$, $\omega_z = 1$, $a = 85a_0/l$, and $l = 0.6075$.

The linear dipole-mode oscillation of a quasi-1D dipolar supersolid in the x direction is more explicitly illustrated in terms of a contour plot of densities $|\psi(x, y, 0)|^2$ (left side) and $|\psi(x, 0, z)|^2$ (right side) as displayed in Fig. 1 at times $t = 0$ [Fig. 1(a)], $t = 7.95$ [Fig. 1(b)], $t = 15.9$ [Fig. 1(c)], $t = 23.85$ [Fig. 1(d)], $t = 31.8$ [Fig. 1(e)], and $t = 39.75$ [Fig. 1(f)]. At $t = 0$ the center of the supersolid lies at $x = 0$, at $t = 7.95$ it moves to the center of the displaced trap at $x = 5$, and at $t = 15.9$ it moves to the position of largest displacement at $x = 10$. After that the supersolid turns around and passes through the center of the displaced trap again at $t = 23.85$ to the initial equilibrium position at $t = 31.8$ at the end of a complete period. Then the system starts to repeat the same cycle again, passing through the center of the displaced trap at $t = 39.75$. This dipole-mode oscillation is found to be simple harmonic with the present amplitude of 5.

Next we consider the linear dipole-mode oscillation of a quasi-2D nine-droplet supersolid of $60\,000$ ^{164}Dy atoms arranged on a square lattice in trap A with angular frequencies $\omega_x = \omega_y = \frac{33}{167}$ and $\omega_z = 1$. The 3D isodensity plot of $|\psi(x, y, z)|^2$ of this supersolid is shown in Figs. 3(a) and 3(b) for densities on contours of 0.0001 and 0.0005, respectively. A background atom cloud surrounding the square-lattice arrangement of nine droplets can be seen clearly in Fig. 3(a). For a large density on the contour in Fig. 3(b), the low-density background atom cloud is not visible and a perfect

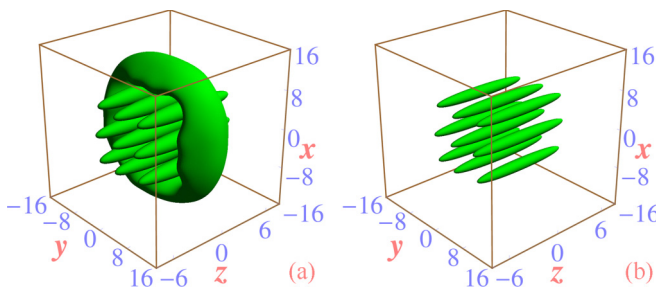


FIG. 3. Three-dimensional isodensity plot of $|\psi(x, y, z)|^2$ of a quasi-2D nine-droplet (square-lattice) supersolid of $N = 60\,000$ ^{164}Dy atoms in trap A with $\omega_x = \omega_y = \frac{33}{167}$ and $\omega_z = 1$ for the value of density on the contour of (a) 0.0001 and (b) 0.0005.

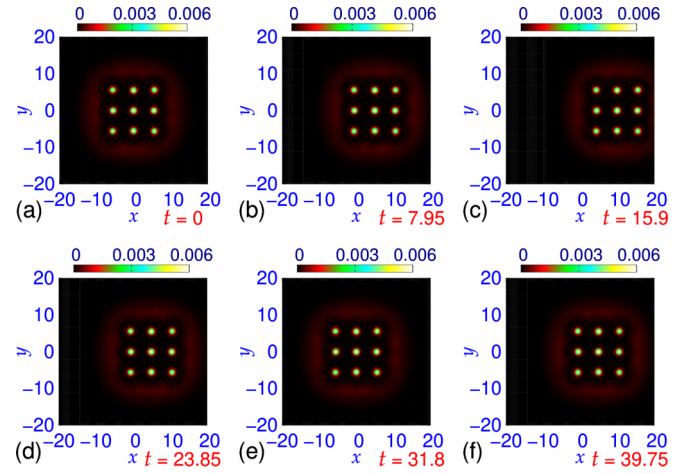


FIG. 4. Contour plot of density $|\psi(x, y, 0)|^2$ of the quasi-2D nine-droplet supersolid of $N = 60\,000$ ^{164}Dy atoms of Fig. 3 executing dipole-mode oscillation in trap A at times (a) $t = 0$, (b) $t = 7.95$, (c) $t = 15.9$, (d) $t = 23.85$, (e) $t = 31.8$, and (f) $t = 39.75$. The trap parameters are $\omega_x = \omega_y = \frac{33}{167}$ and $\omega_z = 1$.

square-lattice arrangement of droplets can be seen. The high-density droplets in a supersolid are embedded in the low-density atom cloud and thus the whole supersolid is phase coherent, which is responsible for frictionless flow and transportability of the supersolid. A similar background atom cloud also exists in a quasi-1D dipolar supersolid. The dipole-mode oscillation of the quasi-2D nine-droplet dipolar supersolid is initiated by displacing the trap through a distance of $x_0 = 5$ units [see Eq. (14)] and studied by real-time propagation using the stationary wave function as the initial state. The time evolution of the position of this quasi-2D supersolid is the same as the quasi-1D supersolid as shown in Fig. 2(a). The time evolution of the energy of this quasi-2D supersolid is distinct from that of the quasi-1D supersolid [see Fig. 2(b)], although both are controlled by the axial trap frequency in the x direction ω_x . The dipole-mode oscillation in the x direction is better illustrated by snapshots of a contour plot of density $|\psi(x, y, 0)|^2$ in the x - y plane at different times $t = 0, 7.95, 15.9, 23.85, 31.8,$ and 39.75 as displayed in Figs. 4(a)–4(f), respectively. The nine-droplet supersolid starts the oscillation in Fig. 4(a), passes through the position of the minimum of trapping potential at $x = 5$ in Fig. 4(b) at $t = 7.95$ to the position of maximum displacement $x = 10$ in Fig. 4(c) at $t = 15.9$. Then it turns around, passes through the position $x = 5$ in Fig. 4(d) at $t = 23.85$ to the initial position $x = 0$ in Fig. 4(e) at $t = 31.8$ and repeats the same dynamics. Although not explicitly demonstrated in this paper, similar oscillation of a hexagonal supersolid was also found. Sustained dipole-mode oscillation without distortion of both the quasi-1D and quasi-2D dipolar supersolids guarantees superfluidity and robustness of the crystalline structure.

B. Scissors-mode oscillation of a quasi-1D supersolid

We consider the quasi-1D dipolar supersolid of a few (three or five) droplets in trap A, with $\omega_x = \frac{33}{167}$ and $\omega_z = 1$, and

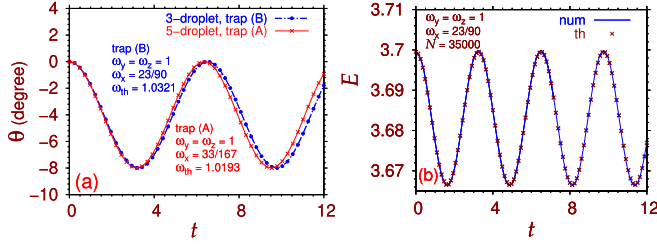


FIG. 5. (a) Angular displacement θ versus dimensionless time t of a quasi-1D three-droplet (five-droplet) supersolid of $N = 35\,000$ ($40\,000$) ^{164}Dy atoms executing scissors-mode oscillation in trap B (A) fitted to the sinusoidal oscillation $\cos(0.935\omega_{\text{th}}t)$ [$\cos(0.971\omega_{\text{th}}t)$] [67,71]. The oscillation is started by giving a rotation of $\theta_0 = -4^\circ$ of the trapping potential at $t = 0$ [see Eq. (15)]. (b) Energy E versus time t plot during the scissors-mode oscillation of the three-droplet supersolid in trap B fitted to the sinusoidal oscillation $\cos(2 \times 0.935\omega_{\text{th}}t)$. For trap A, $\omega_x = \frac{33}{167}$ and $\omega_y = \omega_z = 1$, and for trap B, $\omega_x = \frac{23}{90}$ and $\omega_y = \omega_z = 1$. In trap B the unit of length is $l = 0.8275$.

trap B, with $\omega_x = \frac{23}{90}$ and $\omega_z = 1$. In both cases we study the variation of the scissors-mode-oscillation frequency with a variation of ω_y . By varying ω_y from a small ($\omega_y \ll 1$) to a large ($\omega_y \gg 1$) value we will pass from a quasi-2D trap to a quasi-1D trap and study scissors-mode oscillation of a quasi-1D supersolid in both types of trap. The initial configuration in all calculations is the stationary state obtained by imaginary-time propagation in the appropriate trap, and the angular scissors-mode oscillation is started by rotating the spatially asymmetric harmonic trap in the x - y plane (11) in the z direction in a counterclockwise sense at $t = 0$ through an angle $\theta_0 = -4^\circ$ at $t = 0$ [see (15)] and the subsequent dynamics is studied by real-time simulation. Due to the strong spatial asymmetry ($\omega_y \gg \omega_x$) of the trap in the x - y plane, the dipolar supersolid will execute sustained scissors-mode oscillation [67,76,77] in the z direction. A reasonably large spatial asymmetry of the trap in the x - y plane is necessary for a sustained scissors-mode oscillation [67]. The theoretical frequency of this oscillation for a large superfluid BEC with a Thomas-Fermi distribution of matter is $\omega_{\text{th}} = \sqrt{\omega_x^2 + \omega_y^2}$ [65,67]. Nevertheless, a supersolid with a highly circularly asymmetric distribution of matter, i.e., the droplets and the background atom cloud, has a slightly reduced anomalous moment of inertia compared to the classical moment of inertia and a reduced scissors-mode-oscillation frequency compared to its theoretical estimate.

We consider a quasi-1D three-droplet supersolid in trap B and vary ω_y in the range from $\frac{46}{90}$ to $\frac{110}{90}$. In Figs. 5(a) and 5(b) we illustrate the corresponding time evolution of angle θ and energy E for $\omega_x = \frac{23}{90}$, $\omega_y = \omega_z = 1$, and $N = 35\,000$ fitted to the periodic oscillations $\cos(0.935\omega_{\text{th}}t)$ and $\cos(2 \times 0.935\omega_{\text{th}}t)$, respectively, yielding the frequency $\omega_{\text{sci}} = 0.935\omega_{\text{th}}$ of scissors-mode oscillation with the theoretical frequency $\omega_{\text{th}} = 1.032\,137\,899$. Both the energy and the angle of the oscillating supersolid are found to execute a steady sinusoidal oscillation as shown in Figs. 5(a) and 5(b). The period of angular oscillation $T = 2\pi/\omega_{\text{sci}} = 6.5$ compares well with the theoretical period $T_{\text{th}} = 2\pi/\omega_{\text{th}} = 6.0875$.

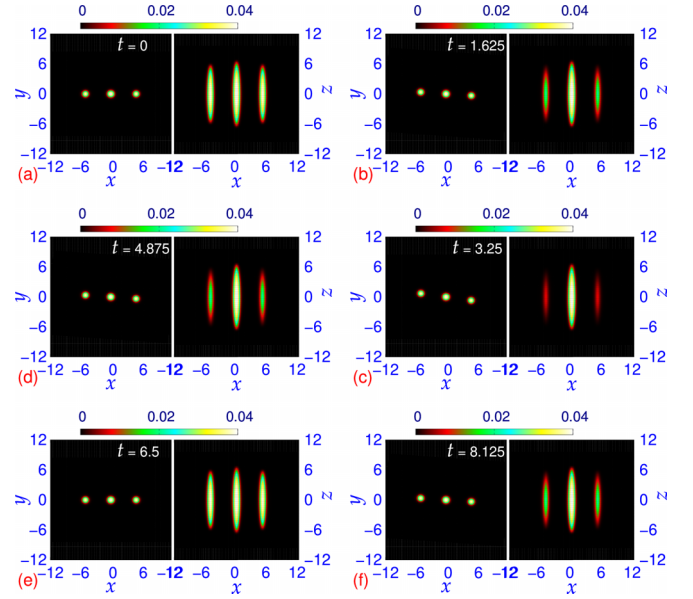


FIG. 6. Contour plot of density $|\psi(x, y, 0)|^2$ (left side of each panel) and $|\psi(x, 0, z)|^2$ (right side of each panel) of the quasi-1D three-droplet supersolid of $N = 35\,000$ ^{164}Dy atoms in trap B of Fig. 5 executing scissors-mode oscillation at times (a) $t = 0$, (b) $t = 1.625$, (c) $t = 3.25$, (d) $t = 4.875$, (e) $t = 6.5$, and (f) $t = 8.125$. For trap B, $\omega_x = \frac{23}{90}$ and $\omega_y = \omega_z = 1$.

The angular oscillation of the supersolid is explicitly displayed in Fig. 6 through a contour plot of densities $|\psi(x, y, z = 0)|^2$ and $|\psi(x, y = 0, z)|^2$ at times $t = 0, 1.625, 3.25, 4.875, 6.5, 8.125$. The supersolid starts to rotate in the clockwise direction at $\theta = 0$ and $t = 0$ [see Fig. 6(a)] and passes through the minimum-energy equilibrium position in the rotated trap at $\theta = -4^\circ$ and $t = 1.625$ [see Fig. 6(b)] to the position of maximum angular displacement of $\theta = -8^\circ$ at $t = 3.25$ [see Fig. 6(c)]. Then the supersolid turns around and again passes through the equilibrium position of $\theta = -4^\circ$ at $t = 4.875$ [see Fig. 6(d)] to the initial position of minimum angular displacement of $\theta = 0^\circ$ at $t = 6.5$ [see Fig. 6(e)] at the end of a complete oscillation. The supersolid then turns around again and the same dynamics is repeated thereafter [see Fig. 6(f)]. At the position of maximum angular displacement of $\theta = -8^\circ$ at $t = 3.25$, two droplets away from the center of the quasi-1D supersolid completely move out of the x - z plane and hence only the central droplet is clearly visible in this plane [see Fig. 6(c)]. For a small angular rotation of the trap in the x - y plane, this angular oscillation should be simple harmonic [67]. The dynamics of angular displacement θ and energy of the quasi-1D supersolid in Figs. 5(a) and 5(b) are found to be simple harmonic for the relatively large spatial trap anisotropy ($\omega_x = \frac{23}{90}$ and $\omega_y = 1$) and a moderate angular amplitude of 4° employed in this study. For a large angle of rotation of the trap $|\theta_0| \gtrsim 8^\circ$ the dynamics ceases to be simple harmonic in nature with a single frequency.

Next we consider the scissors-mode oscillation of a quasi-1D five-droplet supersolid in trap A for $\omega_x = \frac{33}{167}$, $\omega_y = \omega_z = 1$, and $N = 40\,000$ for an initial trap rotation of $\theta_0 = -4^\circ$ in detail. (The same for a three-droplet supersolid

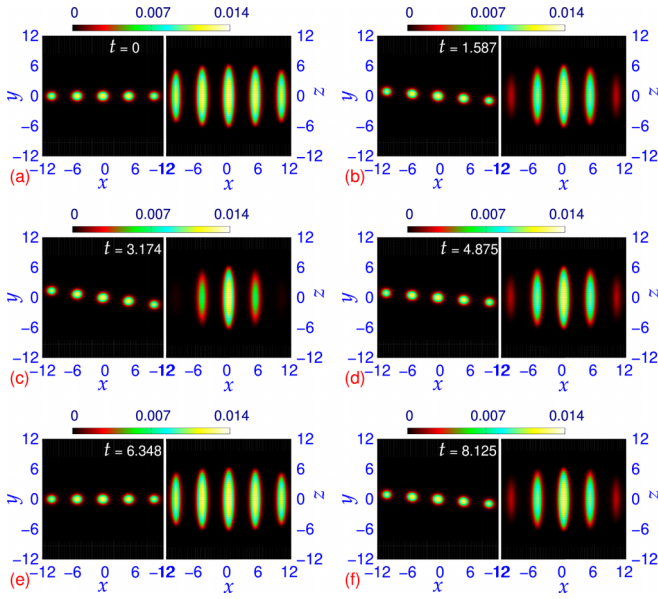


FIG. 7. Contour plot of density $|\psi(x, y, 0)|^2$ (left side of each panel) and $|\psi(x, 0, z)|^2$ (right side of each panel) of a quasi-1D five-droplet supersolid of $N = 40\,000$ ^{164}Dy atoms of Fig. 5 in trap A executing scissors-mode oscillation at times (a) $t = 0$, (b) $t = 1.625$, (c) $t = 3.25$, (d) $t = 4.875$, (e) $t = 6.5$, and (f) $t = 8.125$. For trap A, $\omega_x = \frac{33}{167}$ and $\omega_y = \omega_z = 1$.

in trap A will not be considered here.) The variation of θ with time is illustrated in Fig. 5(a) and fitted to a sinusoidal oscillation. The evolution of this oscillation with time is illustrated by snapshots of contour density plots of $|\psi(x, y, 0)|^2$ and $|\psi(x, 0, z)|^2$ in Fig. 7 at times $t = 0$ [Fig. 7(a)], $t = 1.587$ [Fig. 7(b)], $t = 3.174$ [Fig. 7(c)], $t = 4.875$ [Fig. 7(d)], $t = 6.348$, [Fig. 7(e)], and $t = 8.125$ [Fig. 7(f)] with angular displacements $\theta = 0$, $\theta \approx -4^\circ$, $\theta \approx -8^\circ$, $\theta \approx -4^\circ$, $\theta \approx 0$, and $\theta \approx 4^\circ$, respectively, illustrating the periodic nature of the oscillation. The period of this oscillation is $T = 6.348$, compared to the theoretical period of $T = 2\pi/\omega_{\text{th}} = 6.1634$, and the system is back to the initial state $\theta \approx 0$ in Fig. 7(e) at the end of a complete cycle.

The variation of the frequency of scissors-mode oscillation ω_{sci} of a quasi-1D three-droplet supersolid in trap A or trap B and of a quasi-1D five-droplet supersolid in trap A as a function of frequency ω_y is illustrated in Fig. 8(a) and is compared with the theoretical frequency ω_{th} . The deviation of the scissors-mode-oscillation frequency ω_{sci} from the theoretical frequency ω_{th} , e.g., $\omega_{\text{sci}}/\omega_{\text{th}}$, for different ω_y is presented in Fig. 8(b). The actual scissors-mode frequency is always less [66] than its theoretical estimate $\omega_{\text{th}} > \omega_{\text{sci}}$, as can be found in Fig. 8. The theoretical frequency ω_{th} in both traps leads essentially to the same line shown in Fig. 8(a). Although the theoretical frequency ω_{th} is a good approximation of the actual frequency ω_{sci} for a wide range of variation of trap parameters, as can be seen in Fig. 8(a), the agreement improves as ω_y increases, resulting in an increase of the asymmetry of the trap in the x - y plane. For the same trap, viz., trap A, the agreement improves as the number of droplets increases, resulting in a larger supersolid. For the same frequency ω_y , the agreement also improves in a stronger trap, e.g., trap A with an

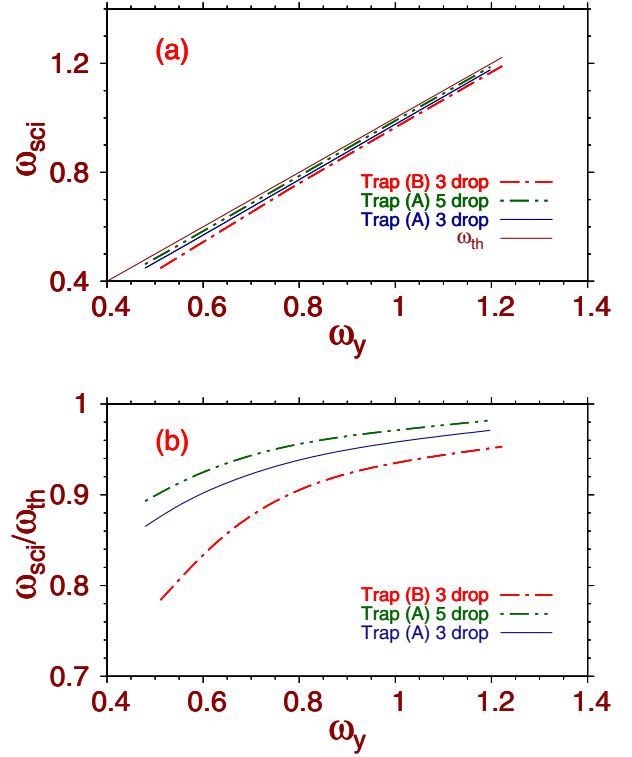


FIG. 8. (a) Frequency of scissors-mode oscillation ω_{sci} versus ω_y for the three- and five-droplet states in trap A and for the three-droplet state in trap B, of amplitude 4° , compared with the theoretical frequency ω_{th} . (b) Deviation of scissors-mode-oscillation frequency from the theoretical frequency $\omega_{\text{sci}}/\omega_{\text{th}}$ versus ω_y for the three- and five-droplet states in trap A and for the three-droplet state in trap B. In trap A $N = 25\,000$ for three droplets and $N = 40\,000$ for five droplets with $\omega_x = \frac{33}{167}$, $\omega_z = 1$, and $\theta_0 = -4^\circ$ and in trap B $N = 35\,000$ for three droplets with $\omega_x = \frac{23}{90}$, $\omega_z = 1$, and $\theta_0 = -4^\circ$.

overall stronger trapping (large $\sqrt[3]{\omega_x \omega_y \omega_z}$) compared to trap B. Nevertheless, for the same number of droplets, the frequency of scissors-mode oscillation was found to be independent of the number of atoms. The trap B is the same as in Ref. [65] and it is possible to compare the present results obtained in trap B with that reference. In trap B, with $\omega_x = \frac{23}{90} = 0.2556$, $\omega_y = \frac{46}{90} = 0.5111$, $\omega_z = 1$, and $a = 87.2a_0$ ($\varepsilon_{\text{dd}} = 1.5$), the experiment in [65] obtained $\omega_{\text{sci}}/\omega_{\text{th}} \approx 0.78 \pm 0.03$. For the same trap with $a = 85a_0$ we get $\omega_{\text{sci}}/\omega_{\text{th}} \approx 0.784$. We also repeated our calculation in the same trap for $a = 87.2a_0$ as in Ref. [65] and we found $\omega_{\text{sci}}/\omega_{\text{th}} = 0.795$, in good agreement with the result in [65]. We also compared the present results with Ref. [66] for $a = 85a_0$, where the trap frequencies $\omega_x = \frac{20}{80} = 0.25$, $\omega_y = \frac{40}{80} = 0.5$, and $\omega_z = 1$ were used, which are pretty close to the present frequencies for trap B in dimensionless units. The result of $\omega_{\text{sci}}/\omega_x \approx 1.74$ in [66] for $a = 85a_0$ translates to $\omega_{\text{sci}}/\omega_{\text{th}} \equiv \omega_{\text{sci}}/\sqrt{\omega_x^2 + \omega_y^2} \approx 0.778$, in good agreement with the present result $\omega_{\text{sci}}/\omega_{\text{th}} \approx 0.784$. In Fig. 8 $\omega_y \gtrsim 0.5$ typically represents a quasi-1D trap and it is also the region of sustained periodic scissors-mode oscillation. As ω_y decreases below a lower limit or increases above an upper limit the scissors-mode oscillation ceases to be simple harmonic with a single frequency and becomes irregular

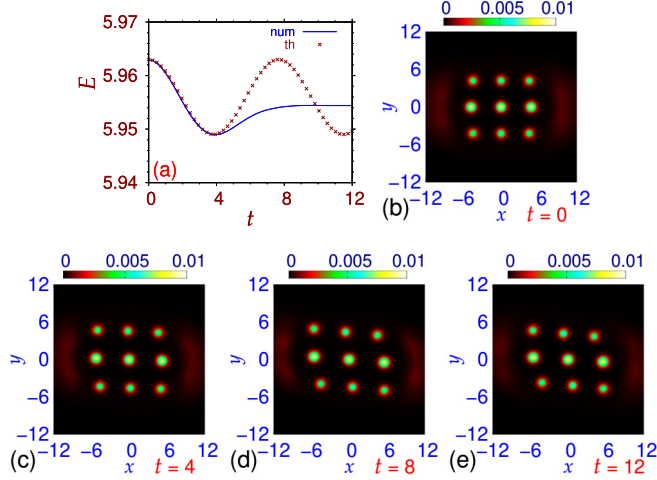


FIG. 9. (a) Numerical (num) energy E versus time t during scissors-mode oscillation of a nine-droplet supersolid of ^{164}Dy atoms of amplitude 4° in trap A fitted to its theoretical estimate (th) $\cos(2 \times \omega_{\text{th}} t)$. Contour plot of the density $|\psi(x, y, 0)|^2$ of this supersolid undergoing scissors-mode oscillation at times (b) $t = 0$, (c) $t = 4$, (d) $t = 8$, and (e) $t = 12$. The parameters for this simulation are $\omega_x = \frac{33}{167}$, $\omega_y = \frac{60}{167}$, $\omega_z = 1$, and $N = 60\,000$.

in nature. The domain of frequencies $0.4 \lesssim \omega_y \lesssim 1.2$ seems to be appropriate for a sustained periodic scissors-mode oscillation. A quasi-2D supersolid can be formed for $\omega_y \lesssim 0.4$, while the trap approximates a quasi-2D configuration; however, in this region one cannot have a sustained scissors-mode oscillation as the trap anisotropy in the x - y plane is smaller than that required for a sustained oscillation. This is why we could not find any scissors-mode oscillation for a quasi-2D supersolid with square or hexagonal symmetry.

To illustrate the breakdown of scissors-mode oscillation for a quasi-2D supersolid explicitly, we consider a quasi-2D nine-droplet supersolid for $\omega_x = \frac{33}{167}$, $\omega_y = \frac{60}{167} \approx 0.359\,28$, $\omega_z = 1$, and $N = 60\,000$. Although a smaller ω_y is favored for the formation of a quasi-2D nine-droplet supersolid, no regular simple-harmonic scissors-mode oscillation could be found there. In this case, for a trap-rotation angle of $\theta_0 = -4^\circ$, the evolution of energy is compared to its theoretical estimate $\cos(2\omega_{\text{th}}t)$ in Fig. 9(a), where there is no periodic oscillation, indicating a breakdown of the scissors-mode oscillation, which can be seen more explicitly from the contour plot of density $|\psi(x, y, 0)|^2$ at times $t = 0$ [Fig. 9(b)], $t = 4$ [Fig. 9(c)], $t = 8$ [Fig. 9(d)], and $t = 12$ [Fig. 9(e)]. Due to a stronger trap in the y direction, the $y = 0$ droplets are larger, accommodating a larger number of atoms than the $y \neq 0$ droplets, as can be seen in the initial density in Fig. 9(b). In Fig. 9(a) we see that the oscillation agrees with the theoretical estimate up to $\frac{1}{4}$ cycle and after this the oscillation becomes irregular. At $t = 4$ in Fig. 9(c), at the end of $\frac{1}{4}$ cycle, the supersolid rotated about 4° . After that the rotation angle increases to about 6° at $t = 8$ in Fig. 9(d) and remains roughly the same thereafter, viz., $t = 12$ in Fig. 9(e), indicating a breakdown of the scissors-mode oscillation.

We also studied the scissors-mode oscillation of a seven-droplet triangular-lattice supersolid state in trap A for

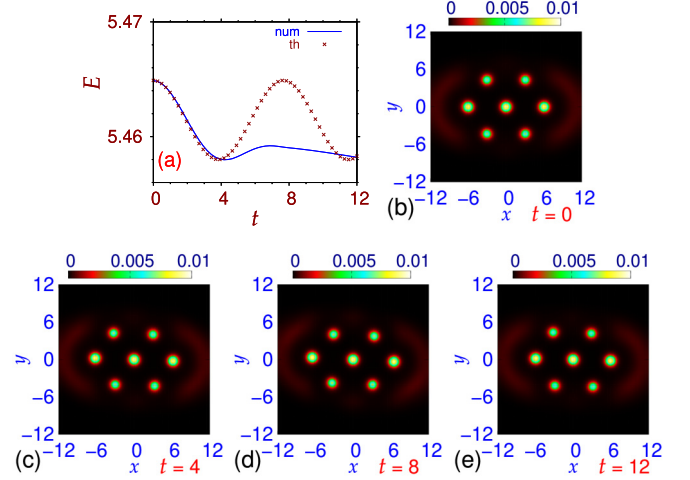


FIG. 10. (a) Numerical (num) energy E versus time t during scissors-mode oscillation of a seven-droplet supersolid of $N = 50\,000$ ^{164}Dy atoms of amplitude 4° in trap A, with $\omega_y = \frac{60}{167}$, fitted to its theoretical estimate (th) $\cos(2 \times \omega_{\text{th}} t)$. Contour plot of the density $|\psi(x, y, 0)|^2$ of this supersolid undergoing scissors-mode oscillation at times (b) $t = 0$, (c) $t = 4$, (d) $t = 8$, and (e) $t = 12$.

$N = 50\,000$ ^{164}Dy atoms. In this case the panorama is quite similar to the case studied in Fig. 9, as exhibited in Fig. 10 through the evolution of energy [Fig. 10(a)] and the contour plot of density $|\psi(x, y, 0)|^2$ at times $t = 0$ [Fig. 10(b)], $t = 4$ [Fig. 10(c)], $t = 8$ [Fig. 10(d)], and $t = 12$ [Fig. 10(e)]. Again, a lack of periodic oscillation in energy in Fig. 10(a) indicates a breakdown of the scissors-mode oscillation. The oscillation is regular up to $t = 4$ [see Fig. 10(c)], where the angular displacement of the supersolid is 4° . After that the angular displacement increases to about 5° and the oscillation practically stops there [see Figs. 10(d) and 10(e)], as in the case of the nine-droplet supersolid in Fig. 9. Similar results were also found in related studies [78,79]. The breakdown of scissors-mode oscillation in these cases of a quasi-2D dipolar supersolid does not mean a lack of superfluidity, because the confining trap does not have a large asymmetry in the x - y plane as required for a sustained scissors-mode oscillation.

IV. SUMMARY

In this paper we studied the linear dipole-mode and angular scissors-mode oscillation dynamics of a dipolar supersolid using a beyond-mean-field model including the LHY interaction with a view to test both the superfluidity and the rigid solid structure of the material. The LHY interaction has a higher-order quartic nonlinear term compared to the cubic nonlinear term of the mean-field model. The quartic nonlinearity leads to a higher-order short-range repulsion that stops the collapse instability resulting from the strong dipolar attraction in the presence of a moderate short-range repulsion resulting from the cubic nonlinear term. In the case of dipole-mode oscillation, both the quasi-1D and quasi-2D supersolids performed exceedingly well on the above-mentioned test, demonstrating the superfluidity and rigid solid structure of the supersolid. Only the quasi-1D dipolar supersolid was capable of executing a stable angular scissors-mode oscillation without any

deformation of the crystalline structure in a highly asymmetric trap in the x - y plane. The relatively large asymmetry of the trap is also necessary for a sustained angular scissors-mode oscillation of a nondipolar BEC. However, in such a trap, it is not possible to have a quasi-2D supersolid; a quasi-2D supersolid naturally appears in a trap with small asymmetry in the x - y plane, but such a trap was found to be not appropriate for a sustained angular scissors-mode oscillation.

In the study of linear dipole-mode oscillation, we considered a quasi-1D three-droplet supersolid and a quasi-2D nine-droplet supersolid in trap A [25,26]. The study of angular scissors-mode oscillation was performed with a quasi-1D three-droplet and a five-droplet supersolid in trap A and with a quasi-1D three-droplet supersolid in trap B with appropriate parameters. The dipole-mode oscillation was started by giving an initial displacement of $x_0 = 5$ of the trap in the x direction perpendicular to the polarization direction z . The angular scissors-mode oscillation was started with an initial rotation of the trap by $\theta_0 = -4^\circ$ around the z axis. For a periodic scissors-mode oscillation, the trap should be asymmetric in the x - y plane with a moderate anisotropy between upper and lower limits. The frequency of the dipole-mode oscillation was found to be identical to the theoretical frequency ω_x in all cases; that of the scissors-mode oscillation was close to, but always less than, its theoretical estimate ω_{th} , as found also in other studies [65,66]. The deviation of the scissors-mode frequency from its theoretical estimate

decreases as the asymmetry of the trap in the x - y plane increased and also as the overall strength of the trap increased from trap B to trap A. The frequency of the scissors-mode oscillation was found to be independent of the number of atoms for a fixed number of droplets in the supersolid but increased with the number of droplets in the supersolid. For the same atomic interaction parameters (a and a_{dd}) and trap frequencies, the present results for scissors-mode frequency are in excellent agreement with those of Refs. [65,66]. The present study of scissors-mode oscillation is complementary to that of Refs. [65,66], where the authors studied the effect of the variation of the atomic interaction on the scissors-mode oscillation. In this paper we studied the effect of the variation of the trap parameters and the number of atoms and droplets on the scissors-mode oscillation. Specifically, we studied the evolution of the scissors-mode oscillation with a variation of the angular frequency ω_y in the y direction, while the trap passes from a quasi-1D to a quasi-2D type. The results of the present study can readily be tested using the experimental setup of Ref. [65].

ACKNOWLEDGMENTS

S.K.A. acknowledges support from the CNPq (Brazil) Grant No. 301324/2019-0. The use of the supercomputing cluster of the Universidad de Cartagena is acknowledged.

-
- [1] E. P. Gross, *Phys. Rev.* **106**, 161 (1957).
 [2] A. F. Andreev and I. M. Lifshitz, *Zh. Eksp. Teor. Fiz.* **56**, 2057 (1969) [*Sov. Phys. JETP* **29**, 1107 (1969)].
 [3] A. J. Leggett, *Phys. Rev. Lett.* **25**, 1543 (1970).
 [4] G. V. Chester, *Phys. Rev. A* **2**, 256 (1970).
 [5] M. Boninsegni and N. V. Prokofev, *Rev. Mod. Phys.* **84**, 759 (2012).
 [6] V. I. Yukalov, *Physics* **2**, 49 (2009).
 [7] E. Kim and M. H. W. Chan, *Nature (London)* **427**, 225 (2004).
 [8] S. Balibar, *Nature (London)* **464**, 176 (2010).
 [9] F. Cinti, T. Macrì, W. Lechner, G. Pupillo, and T. Pohl, *Nat. Commun.* **5**, 3235 (2014).
 [10] Z.-K. Lu, Y. Li, D. S. Petrov, and G. V. Shlyapnikov, *Phys. Rev. Lett.* **115**, 075303 (2015).
 [11] N. Y. Yao, C. R. Laumann, A. V. Gorshkov, S. D. Bennett, E. Demler, P. Zoller, and M. D. Lukin, *Phys. Rev. Lett.* **109**, 266804 (2012).
 [12] F. Wächtler and L. Santos, *Phys. Rev. A* **93**, 061603(R) (2016).
 [13] Y. Li, G. I. Martone, L. P. Pitaevskii, and S. Stringari, *Phys. Rev. Lett.* **110**, 235302 (2013).
 [14] L. Chomaz, D. Petter, P. Ilzhöfer, G. Natale, A. Trautmann, C. Politi, G. Durastante, R. M. W. van Bijnen, A. Patscheider, M. Sohmen, M. J. Mark, and F. Ferlaino, *Phys. Rev. X* **9**, 021012 (2019).
 [15] L. Tanzi, E. Lucioni, F. Famà, J. Catani, A. Fioretti, C. Gabbanini, R. N. Bisset, L. Santos, and G. Modugno, *Phys. Rev. Lett.* **122**, 130405 (2019).
 [16] M. Guo, F. Böttcher, J. Hertkorn, J.-N. Schmidt, M. Wenzel, H. P. Büchler, T. Langen, and T. Pfau, *Nature (London)* **574**, 386 (2019).
 [17] L. Tanzi, S. Rocuzzo, E. Lucioni, F. Famà, A. Fioretti, C. Gabbanini, G. Modugno, A. Recati, and S. Stringari, *Nature (London)* **574**, 382 (2019).
 [18] M. A. Norcia, C. Politi, L. Klaus, E. Poli, M. Sohmen, M. J. Mark, R. Bisset, L. Santos, and F. Ferlaino, *Nature (London)* **596**, 357 (2021).
 [19] J.-R. Li, J. Lee, W. Huang, S. Burchesky, B. Shteynas, F. Ç. Top, A. O. Jamison, and W. Ketterle, *Nature (London)* **543**, 91 (2017).
 [20] J. Léonard, A. Morales, P. Zupancic, T. Esslinger, and T. Donner, *Nature (London)* **543**, 87 (2017).
 [21] S. K. Adhikari, *Phys. Rev. A* **103**, L011301 (2021).
 [22] S. K. Adhikari, *J. Phys.: Condens. Matter* **33**, 265402 (2021).
 [23] P. Kaur, S. Gautam, and S. K. Adhikari, *Phys. Rev. A* **105**, 023303 (2022).
 [24] S. K. Adhikari, *J. Phys.: Condens. Matter* **33**, 425402 (2021).
 [25] H. Kadau, M. Schmitt, M. Wenzel, C. Wink, T. Maier, I. Ferrier-Barbut, and T. Pfau, *Nature (London)* **530**, 194 (2016).
 [26] M. Schmitt, M. Wenzel, F. Böttcher, I. Ferrier-Barbut, and T. Pfau, *Nature (London)* **539**, 259 (2016).
 [27] L. Chomaz, S. Baier, D. Petter, M. J. Mark, F. Wächtler, L. Santos, and F. Ferlaino, *Phys. Rev. X* **6**, 041039 (2016).
 [28] F. Wächtler and L. Santos, *Phys. Rev. A* **94**, 043618 (2016).
 [29] R. N. Bisset, R. M. Wilson, D. Baillie, and P. B. Blakie, *Phys. Rev. A* **94**, 033619 (2016).
 [30] I. Ferrier-Barbut, H. Kadau, M. Schmitt, M. Wenzel, and T. Pfau, *Phys. Rev. Lett.* **116**, 215301 (2016).
 [31] G. Natale, R. M. W. van Bijnen, A. Patscheider, D. Petter, M. J. Mark, L. Chomaz, and F. Ferlaino, *Phys. Rev. Lett.* **123**, 050402 (2019).

- [32] F. Böttcher, J.-N. Schmidt, M. Wenzel, J. Hertkorn, M. Guo, T. Langen, and T. Pfau, *Phys. Rev. X* **9**, 011051 (2019).
- [33] R. Bombin, J. Boronat, and F. Mazzanti, *Phys. Rev. Lett.* **119**, 250402 (2017).
- [34] J. Hertkorn, J.-N. Schmidt, M. Guo, F. Böttcher, K. S. H. Ng, S. D. Graham, P. Uerlings, T. Langen, M. Zwierlein, and T. Pfau, *Phys. Rev. Res.* **3**, 033125 (2021).
- [35] Y.-C. Zhang, F. Maucher, and T. Pohl, *Phys. Rev. Lett.* **123**, 015301 (2019).
- [36] E. Poli, T. Bland, C. Politi, L. Klaus, M. A. Norcia, F. Ferlaino, R. N. Bisset, and L. Santos, *Phys. Rev. A* **104**, 063307 (2021).
- [37] D. Baillie and P. B. Blakie, *Phys. Rev. Lett.* **121**, 195301 (2018).
- [38] Y.-C. Zhang, T. Pohl, and F. Maucher, *Phys. Rev. A* **104**, 013310 (2021).
- [39] L. E. Young-S. and S. K. Adhikari, *Phys. Rev. A* **105**, 033311 (2022).
- [40] L. E. Young-S. and S. K. Adhikari, *Eur. Phys. J. Plus* **137**, 1153 (2022).
- [41] J. Hertkorn, J.-N. Schmidt, M. Guo, F. Böttcher, K. S. H. Ng, S. D. Graham, P. Uerlings, H. P. Büchler, T. Langen, M. Zwierlein, and T. Pfau, *Phys. Rev. Lett.* **127**, 155301 (2021).
- [42] J. Metz, T. Lahaye, B. Fröhlich, A. Griesmaier, T. Pfau, H. Saito, Y. Kawaguchi, and M. Ueda, *New J. Phys.* **11**, 055032 (2009).
- [43] T. D. Lee, K. Huang, and C. N. Yang, *Phys. Rev.* **106**, 1135 (1957).
- [44] A. R. P. Lima and A. Pelster, *Phys. Rev. A* **84**, 041604(R) (2011).
- [45] R. Schützhold, M. Uhlmann, Y. Xu, and U. R. Fischer, *Int. J. Mod. Phys. B* **20**, 3555 (2006).
- [46] F. Böttcher, J.-N. Schmidt, J. Hertkorn, K. S. H. Ng, S. D. Graham, M. Guo, T. Langen, and T. Pfau, *Rep. Prog. Phys.* **84**, 012403 (2021).
- [47] E. J. Halperin, S. Ronen, and J. L. Bohn, *Phys. Rev. A* **107**, L041301 (2023).
- [48] P. Ilzhöfer, M. Sohmen, G. Durastante, C. Politi, A. Trautmann, G. Natale, G. Morpurgo, T. Giamarchi, L. Chomaz, M. J. Mark, and F. Ferlaino, *Nat. Phys.* **17**, 356 (2021).
- [49] G. Semeghini, G. Ferioli, L. Masi, C. Mazzinghi, L. Wolswijk, F. Minardi, M. Modugno, G. Modugno, M. Inguscio, and M. Fattori, *Phys. Rev. Lett.* **120**, 235301 (2018).
- [50] C. R. Cabrera, L. Tanzi, J. Sanz, B. Naylor, P. Thomas, P. Cheiney, and L. Tarruell, *Science* **359**, 301 (2018).
- [51] D. S. Petrov, *Phys. Rev. Lett.* **115**, 155302 (2015).
- [52] P. B. Blakie, D. Baillie, L. Chomaz, and F. Ferlaino, *Phys. Rev. Res.* **2**, 043318 (2020).
- [53] M. N. Tengstrand, D. Boholm, R. Sachdeva, J. Bengtsson, and S. M. Reimann, *Phys. Rev. A* **103**, 013313 (2021).
- [54] T. Bland, E. Poli, L. A. Peña Ardila, L. Santos, F. Ferlaino, and R. N. Bisset, *Phys. Rev. A* **106**, 053322 (2022).
- [55] S. Li, U. Ngoc Le, and H. Saito, *Phys. Rev. A* **105**, L061302 (2022).
- [56] J. Zhang, C. Zhang, J. Yang, and B. Capogrosso-Sansone, *Phys. Rev. A* **105**, 063302 (2022).
- [57] M. Schmidt, L. Lassablière, G. Quémener, and T. Langen, *Phys. Rev. Res.* **4**, 013235 (2022).
- [58] S. Conti, A. Perali, A. R. Hamilton, M. V. Milošević, F. M. Peeters, and D. Neilson, *Phys. Rev. Lett.* **130**, 057001 (2023).
- [59] B. K. Turmanov, B. B. Baizakov, F. K. Abdullaev, and M. Salerno, *J. Phys. B* **54**, 145302 (2021).
- [60] F. Ancilotto, M. Barranco, M. Pi, and L. Reatto, *Phys. Rev. A* **103**, 033314 (2021).
- [61] R. Sachdeva, M. N. Tengstrand, and S. M. Reimann, *Phys. Rev. A* **102**, 043304 (2020).
- [62] S. M. Roccuzzo and F. Ancilotto, *Phys. Rev. A* **99**, 041601(R) (2019).
- [63] J. Hertkorn, F. Böttcher, M. Guo, J. N. Schmidt, T. Langen, H. P. Büchler, and T. Pfau, *Phys. Rev. Lett.* **123**, 193002 (2019).
- [64] I. Ferrier-Barbut, M. Wenzel, F. Böttcher, T. Langen, M. Isoard, S. Stringari, and T. Pfau, *Phys. Rev. Lett.* **120**, 160402 (2018).
- [65] L. Tanzi, J. G. Maloberti, G. Biagioni, A. Fioretti, C. Gabbanini, and G. Modugno, *Science* **371**, 1162 (2021).
- [66] S. M. Roccuzzo, A. Gallemí, A. Recati, and S. Stringari, *Phys. Rev. Lett.* **124**, 045702 (2020).
- [67] D. Guéry-Odelin and S. Stringari, *Phys. Rev. Lett.* **83**, 4452 (1999).
- [68] T. Lahaye, C. Menotti, L. Santos, M. Lewenstein, and T. Pfau, *Rep. Prog. Phys.* **72**, 126401 (2009).
- [69] R. Kishor Kumar, L. E. Young-S., D. Vudragović, A. Balaž, P. Muruganandam, and S. K. Adhikari, *Comput. Phys. Commun.* **195**, 117 (2015).
- [70] V. I. Yukalov, *Laser Phys.* **28**, 053001 (2018).
- [71] M. Modugno, G. Modugno, G. Roati, C. Fort, and M. Inguscio, *Phys. Rev. A* **67**, 023608 (2003).
- [72] V. Lončar, L. E. Young-S., S. Škrbić, P. Muruganandam, S. K. Adhikari, and A. Balaž, *Comput. Phys. Commun.* **209**, 190 (2016).
- [73] L. E. Young-S., P. Muruganandam, A. Balaž, and S. K. Adhikari, *Comput. Phys. Commun.* **286**, 108669 (2023).
- [74] P. Muruganandam and S. K. Adhikari, *Comput. Phys. Commun.* **180**, 1888 (2009).
- [75] Y. Tang, A. Sykes, N. Q. Burdick, J. L. Bohn, and B. L. Lev, *Phys. Rev. A* **92**, 022703 (2015).
- [76] S. M. Roccuzzo, A. Recati, and S. Stringari, *Phys. Rev. A* **105**, 023316 (2022).
- [77] O. M. Maragò, S. A. Hopkins, J. Arlt, E. Hodby, G. Hechenblaikner, and C. J. Foot, *Phys. Rev. Lett.* **84**, 2056 (2000).
- [78] M. A. Norcia, E. Poli, C. Politi, L. Klaus, T. Bland, M. J. Mark, L. Santos, R. N. Bisset, and F. Ferlaino, *Phys. Rev. Lett.* **129**, 040403 (2022).
- [79] A. Gallemí and L. Santos, *Phys. Rev. A* **106**, 063301 (2022).